Lone-pair self-containment in pyritohedron-shaped closed cavities: Optimised hydrothermal synthesis, structure and magnetism of $Co_{15}F_2(TeO_3)_{14}$

Minfeng Lü,[a,*, ID] Jianhua Jiang,[a] Bei Zhu,[a] Yuwei Zhao,[a] Tianyu Zhu,[a] Haoming Yang,[a] Yong Jin, [a] Houria Kabbour,[b] Kwang-Yong Choi[c] and William T. A. Harrison[d,*]

[a] School of Environmental & Chemical Engineering, Jiangsu University of Science and Technology, Zhenjiang 212003, Jiangsu, Perople's Republic of China

[b]Université Lille Nord de France, UMR 8181 CNRS, Unité de Catalyse et de Chimie du Solide (UCCS USTL), F-59655 Villeneuve d'Ascq, France

[c]Department of Physics, Chung-Ang University, 84 Heukseok-ro, Dongjak-gu, Seoul 06974, Republic of Korea

[d] Department of Chemistry, University of Aberdeen, Aberdeen, AB24 3UE, Scotland

*To whom correspondence should be addressed

AUTHOR INFORMATION

Corresponding Author

m.f.lv@hotmail.com (Minfeng Lü), w.harrison@abdn.ac.uk (William T. A. Harrison)

ORCID[ID]

Minfeng Lü: 0000-0003-2576-3840

Acknowledgments

M. L., J. J., B.Z., Y. Z., T. Z., H. Y., and Y. J. acknowledge support from the National Natural Science Foundation of China (Award No. 21671185). H. K. acknowledge support from the Multi-InMaDe project of the ANR, Award No. Grant ANR 2011-JS-08 003 01.

Abstract

The new oxofluoride $Co_{15}F_2(TeO_3)_{14}$ has been prepared by the optimised hydrothermal synthesis. concerned with complex mineralization process and redox chemistry. The crystal structure consists of a three-dimensional network of $CoO_5(O,F)$ octahedra, distorted CoO_5 square pyramids, TeO_3 trigonal pyramids and grossly distorted TeO_{3+3} octahedra, which are linked by sharing corners and edges. The Te(IV) lone pairs are accommodated within novel pyritohedron-shaped $[(TeO_3)_{14}]^{28-}$ units. Magnetic susceptibility data for $Co_{15}F_2(TeO_3)_{14}$ show

antiferromagnetic ordering below 9.6 K with a substantial orbital component to the effective magnetic moment. An *S*=3/2 honeycomblike spin network was carefully analyzed by experimental techniques and first principles calculation.

Keywords: *transition metal oxide fluorides, building units, hydrothermal, single-crystal X-ray diffraction, magnetism,*

1. Introduction

Compounds with multiple anions (more than one anionic species), such as oxyhalides oxynitrides and oxyhydrides, have been attracted attention due to diverse chemistries and structures which may lead to superior functionality.[1] Famous examples are high-*Tc* superconductors LaOFeAs [2] and $Sr_2CuO_2F_2$,[3] the oxynitride semiconductors AMO_2N (A= Ba, Sr, Ca;M= Ta, Nb) [4] and the oxyhydride $BaTiO_{3-x}H_x$[5] which exhibits hydride exchange and electronic conductivity. Tellurites however, possess a rich and varied crystal chemistry because of the unpredictable and irregular coordination geometries adopted by the Te^{IV} atoms, which can bond to between three and six O atoms. This behavior is characteristic of *p*-block cations with ns^2np^0 electronic configurations and may be ascribed to a second-order Jahn−Teller (SOJT) effect,[6–8] which results in a stereochemically-active lone pair of electrons,[9,10] which must be spatially accommodated within the crystal structure. In previous studies, it has been found that the Te lone pairs can form one-dimensional lone-pair channels,[11] where TeO_x (x = 3, 4, 5) polyhedra are connected to MO_y units (M = metal cation) or two-dimensional lone-pair sheets,[12] whose interlayer spacing are large enough to accommodate other chemical species such as alkali-metal cations.[13] However, lone-pair 'self-containments', where extended tellurite topological networks are formed by themselves are rare, with one example being the barium tellurites[14] $BaTe_3O_7$ and $BaTe_4O_9$, which accommodate the Te^{IV} lone pairs in infinite, self-contained, one-dimensional tubes, interspersed by the barium cations.

Recently, transition-metal halo-tellurites and halo-selenites have been investigated as quantum spin systems with interesting magnetic and physical properties. For example, $FeSeO_3F$[16] is composed of alternating antiferromagnetic chains and $FeTe_2O_5Br$ exhibits multiferroicity.[16] These oxohalides can be divided into two categories: the larger halide ions (Cl^- and Br^-) with low coordination numbers act as a terminal ligands, with examples being $FeTe_2O_5X$ (X = Cl, Br),[17] $Cu_2Te_2O_5X_2$,[18] $Ni_5(TeO_3)_4X_2$,[12] $Cu_4Te_5O_{12}Cl_4$[19] and $Fe_3Te_3O_{10}Cl$.[20] On

the other hand, the smaller fluoride anion may act as a bridging species between transition metal cations in phases such as $V_2Te_2O_7F_2$,[21] $MTeO_3F$ (M = Fe, Ga),[22] $Co_2TeO_3F_2$, and $Co_2SeO_3F_2$.[23] It may also be noted that there exist different bonding preferences between the transition metal cation and lone-pair cation. Transition metal cations prefer to bond with both oxygen and halide anions, while lone-pair cations prefer exclusively to coordinate to oxide anions.[10] This suggests that the crystal chemistry in transition metal halo-tellurite systems is governed not only by the asymmetric coordination of Te^{4+} cations but also by bonding preferences of the transition metal ions for oxide and halide anions to form $M(O,X)_n$ polyhedra.

In this short article, we extend multiple anions idea on transition-metal halo-tellurites using the improved hydrothermal synthesis method, in contrast to previous ones via unique mineralizers, i.e hydroxide, metal halide, metal fluorides, we surprised found compound $Co_{15}F_2(TeO_3)_{14}$, **1** features its unique pyritohedron-shaped Te^{IV} lone-pair self-contained cavities, which characterizated by X-ray diffraction and magnetic susceptibility.

2. Experimental section

A mixture of 0.015 mol (1.567 g) RbF (Sigma-Aldrich, 99.8%), 1.50×10^{-4} mol (0.036 g) $CoCl_2 \cdot 6H_2O$ (Energy Chemical, 99%) and 3.75×10^{-4} mol (0.060 g) TeO_2 (Sigma-Aldrich, 99%) was placed in a Teflon-lined stainless steel autoclave (23 ml) with 0.016 ml of hydrazine monohydrate and 1.5 ml of deionized water. The vessel was sealed and heated to 220 °C for 72 hours and cooled slowly (5 °C h^{-1}) to room temperature. After filtering and rinsing with water, blue prismatic single crystals of **1** and polycrystalline metallic Te were recovered. Several attempts have been made to prepare **1** by solid-state reaction but these led to $CoTeO_3$. It should be stressed that tiny ammonium species are rather crucial to the formation of $Co_{15}F_2(TeO_3)_{14}$ phase. $Co_2Te_3O_8$ was mainly found on the condition of 0.008 ml of hydrazine monohydrate, while metallic Te was recovered on the condition of 0.024 ml of hydrazine monohydrate.In deed. Both alikali metal fluoride sources and ammonium species have been used as mineralizers to aid in the formation of $Co_{15}F_2(TeO_3)_{14}$ phase, while ammonium species also play important role of redox process. A single-phase polycrystalline sample of **1** was obtained by manually separating and grinding the single crystals (Figure S1). The cell parameters refined against the X-ray

powder diffraction pattern [a = 11.7067 (5) Å, c= 27.301 (1) Å] are in good agreement with those from the single crystal data, summarized in Table 1.

The SCXRD data were collected on a Bruker SMART BREEZE diffractometer using graphite-monochromatized Mo Ka radiation, λ= 0.71073 Å. Data reduction was carried out with SAINT [24] and a multi-scan absorption correction was performed with SADABS.[25] The crystal structure was solved by direct methods with SHELXS-97 [26] and the model was completed and optimized by refinement against $|F^2|$ using SHELXL-2014.[27] Energy-dispersive analysis by X-ray (EDAX) of the isolated blue crystals was carried out using a Hitachi S-3400N. EDX analyses under the similar process and reported elsewhere,[28,29] which indicated the peaks for Co and F in the EDX analysis were overlapped; however, (Co + F): Te ratio was identified as 16.4:14.6, in agreement with the expected one (Figure S2).

IR spectra were recorded on an Agilent Carry 670-IR FTIR spectrometer in the spectral range 400−4000 cm^{-1}, with an attenuated total reflection (ATR) accessory. The absence of hydrogen-bonded groups (absorption peak at around 3600 cm-1, supported the fact that fluorine (rather than say hydroxide) is part of the structure (Figure S4). UV/Vis/NIR absorption spectra were recorded using a Perkin-Elmer (USA) Lambda 950 UV-Vis-NIR spectrophotometer (Figure S5). TGA were performed using a high-resolution TA Instruments Q50 Thermogravimetric Analyzer. Polycrystalline samples were put into alumina crucibles and heated at a rate of 10 °C min^{-1} from room temperature to 790 °C under flowing nitrogen gas (Figure S6).

The DC magnetic susceptibility of **1** was measured using a Quantum Design Magnetic Properties Measurement System (MPMS). Zero-field-cooled (ZFC) and field-cooled (FC) data were collected in the temperature range 2–320 K under an external field of 200 Oe. The specific heat measurement was collected with the heat capacity option of a physical properties measurement system (PPMS-9, Quantum Design).

Spin-polarized DFT calculations were carried out in the framework of the Vienna ab initio simulation package (VASP) [30-32] using the projector augmented wave (PAW) method and the generalized gradient approximation of Perdew, Burke and Ernzerhof for the exchange-correlation functionals. [33] The plane wave cutoff energy of 400 eV and the threshold of self-consistent-field energy convergence of 10^{-6} eV were used with a set of 5×5×2 k-points. In order to account for the strong electron correlation associated with the 3d states of Cobalt atoms, we employed the DFT plus on-site repulsion U (DFT+U) method as described by Dudarev [34] with

the effective on-site repulsion U_{eff} = U – J = 3-4 eV. For U= 3 eV and U= 4 eV, the results are qualitatively similar with topologies of the DOS mainly conserved, only slightly increased band gap and magnetic moments are found for U= 4 eV. For the PDOS description, we focus on the calculations at U= 4 eV. The electron localization function (ELF) has been also computed and allows the visualization of the nodal structure of the molecular orbital, including Lone Pair electrons. [35]

3. Results and discussion

The crystal structure of **1** contains three distinct Co atoms and three Te atoms, which defines the unusual 15:14 Co to Te stoichiometry in this phase. The location of the fluorine atom at Wyckoff site 6c (0, 0, *z*) is supported by its bond valence sum (BVS) value (in valence units)[36] of –0.96 and by the results of IR, due to the absence of hydrogen-bonded groups (absorption peak at around 3600 cm^{-1}, see Figure S4). The BVS data for the Te (4.03–4.28) and Co (1.81–1.98) atoms confirm their valences to be IV and II, respectively. The coordination geometry around Co1 (site symmetry $\bar{1}$) is a slightly squashed octahedron composed of O atoms from six different tellurite anions (two each of Te1, Te2 and Te3) with two short [2.016 (5) Å] and four elongated [2.154 (5) and 2.165 (3) Å] bonds (Figure 1); the mean separation of 2.112 Å is similar to that observed in $CoSeO_3$ (2.143 Å).[37] In contrast, Co2 is bonded to five O atoms [four with d < 2.07 Å and one with d = 2.339 (3) Å]. The value of 0.40 for the Addison τ parameter[38] for Co2 indicates a geometry intermediate between square-base pyramidal (τ = 0) and trigonal bipyramidal (τ = 1), but slightly closer to the former. The spread of bond lengths about Co2 is similar to those for the cobalt atom in $LaBaCoO_{4.25}$ [1.999 (4)–2.335 (4) Å].[39] The Co3 cation in **1** is bonded to five O atoms and one F atom in a distorted octahedral geometry with distances ranging from 2.040 (5) to 2.175 (4) Å and *cis* bond angles ranging from 77.66 (13) to 105.90 (13)°.

Atom Te1 (site symmetry 3) has three O1 atom near neighbors with Te–O = 1.887 (3) Å and O–Te–O = 98.22 (13)°, defining a pyramidal shape, which is typical for this type of tellurium–oxygen grouping.[40] However, there are also three long Te–O interactions at 2.941 (4) Å [to O4], compared to the van der Waals separation for these atoms of 3.58 Å. We term this coordination geometry TeO_{3+3}:[41,42] the calculated BVS for Te1 increases from 3.84 to 4.06 when

considering all six O atoms. Atom Te2 has three O atoms in close proximity (d < 1.90 Å), to form a more asymmetric trigonal pyramidal coordination environment with an O–Te–O bond angle distribution of 87.3 (2) ‒ 94.67 (16)°. These three O atoms together with three distant O atoms [O4 at 2.655 (4) Å, O6 at 2.742 (4) Å and O6 at 2.850 (4) Å] make up a grossly distorted octahedron around Te2, again leading to a TeO_{3+3} coordination geometry. The Te3 species has three O atom near neighbors in a trigonal pyramidal coordination environment, which are similar to those observed in $KY(TeO_3)_2$.[10] The Te–O bonds lengths range from 1.857 (3) to 1.891 (3) Å with a very narrow distribution of O–Te–O bond angles from 98.47 (15) to 98.97 (15)°.

The oxygen atoms in **1** adopt three kinds of co-ordinations: a) bonds to one Co and two Te in essentially planar conformation (O1, O3, O5 and O7); b) bonds to one Te and three Co in distorted tetrahedral geometry (O2); c) bonds to three Te and one Co in tetrahedral conformation (O4 and O6), where two long Te‒O bonds are needed to form the distorted tetrahedral $O(CoTe_3)$ unit. The unique fluorine atom is connected to three Co3 atoms in essentially planar configuration, hence acting as a bridging species to connect three CoO_5F octahedra. To our best knowledge, one fluoride anion usually bridges two transition metal cations, the connection with three transition-metal cations is quite rare.

It should be mentioned that each Te3 species together with Te1 and Te2 or two Te2 species lead to a six-membered ring containing four long Te–O bonds around Te1/Te2 and two short Te–O bonds around Te3 (Figure 2b). The O4···O6 distance of 2.826 (5) Å in the $Te3O_3$ group is approximately equal to the long Te–O bonds around Te1/Te2, leading to the formation of a slightly distorted pentagonal face if these O4···O6 contacts are deemed to be "bonds", in which case, the Te3 species project out of the pentagonal face. A cluster of twelve of these pentagonal faces meet at 20 vertices [two Te1, six Te2, six O4 and six O6] to generate a distorted pyritohedral cavity (Figure 2a) centered at the point (0, 0, ½) and equivalent locations, where the two short Te3–O bonds can be regarded a "handle" fixed at the edge of O4···O6 "bond" (Figure 2c). Finally, the structural effect of the Te^{IV} lone pairs may be discussed, especially Te1 and Te2: if we assume that the lone pairs for these species occupy the fourth vertex of a tetrahedron then their lone pairs and diagonal counterparts are all directed towards the point (0, 0, ½).In fact, the electron localization function (reference) (ELF) [35] in the DFT (GGA-PBE) calculations allows visualizing the Tellurium atoms lone pairs which are pointing as intuitively described above, as also seen in the Figure S7. Thus the equator of the cavity is formed from a Te2-centred 6-ring,

the hemisphere of the cavity is formed from a trio of $Te3O_3$ groups on the top or bottom, while the polar area of the cavity is formed from the Te1-centred groups (Figure 2a). More importantly, Lone-Pair Self-Containments, where extended tellurite networks are formed by themselves are very rare. This novel way to accommodate Te(IV) lone-pair electrons need unusual Te-O bonds to form untypical polyhedrals. i.e distorted square based pyramid formed by less regular coordination found in $BaTe_3O_7$,[14] while an usual axial Te–O bonds relative to the equatorial bonds found in $BaTe_4O_9$.[14] Coordination geometry TeO_{3+3} with distorted octahedron shape in $Co_{15}F_2(TeO_3)_{14}$ support this Lone-Pair Self-Containments configuration. Besides this, there is structure-directing effect on the position of lone-pair. One-dimensional Lone-Pair Self-Containment of barium tellurites last time is aided by large Ba^{2+}, where Lone-Pair Self-Containments tellurite networks were isolated by one of two large Ba^{2+} .while, Zero-dimensional Lone-Pair Self-Containment of our sample is formed honeycomb-like, Co-centred polyhedra network, pyritohedron-shaped Te(IV) lone-pair cavities are finally sealed trimeric octahedron jointed by a common fluorine atom.

The extended structure of **1** features corner and edge sharing between the Co- and Te-centred polyhedral (Figure 1d). The infinite, honeycomb-like, layered structure may be schematically described in stacking sequence. These sequences include Co3/Te2-centred polyhedron layer, which is characterized as 12 ring of Co3 units and 6 rings of Te2 groups (details see Figure S8), and concomitant Co2/Te3-centred polyhedron layer attached at the top and bottow, followed by Co1/Te1-centred polyhedron layer, and then *another Co2/Te3* -centred polyhedron layer, where the former Co2/Te3 sheets are laterally displaced from each other by x = 1/3 and y = 2/3. Finally, *another Co3/Te2*-centered polyhedron layer with the displacement by x = 1/3 and y = 2/3 from the former ones. Finally, These honeycomb layers fused sequentially to form a continuous, three-dimensional structure, which enclose pyritohedron-shaped Te(IV) lone-pair self-contained cavities. Due to rhombohedral crystal symmetry, there are no continuous channels of any significant size in this structure. [42]

In order to analyze the relationship between structure and properties, we have carried out the DFT (GGA-PBE) calculations on the title phase, leading to a semiconductor electronic structure even without inclusion of a Hubbard term *U, i.e. a band gap is opened* with value of 0.25 eV, while DFT may lead to erratic metallic states as far as *d* electrons are concerned. Within this approximation, the calculated magnetic moments on the different cobalt atoms, *i.e.* the

octahedral CoO_6, the trigonal bipyramid coordinated CoO_5 (TBP), and the heteroleptic (mixed anion) octahedral CoO_5F, are respectively equal to 2.53 μB, 2.53 μB and 2.59 μB. These rather close values are consistent with a high spin Co^{2+} (d^7) configuration on all the distinct Co sites despite the different environments and expected crystal field splitting especially for the TBP [43]. For the later similar high spin states of Co^{2+} have been described for instance in the phase $Co_2(OH)PO_4$ or $Co_2(OH)AsO_4$.[44,45] Then applying a Hubbard term with U= 4 eV led to a reasonable band gap of 2.75 eV (consistant with its blue color) and slightly increased magnetic moments of 2.76 μB, 2.74 μB and 2.77 μB with qualitatively similar character of the electronic structure. We will focus on the results obtained using GGA+U (U= 4 eV) for the rest of the discussion.

The projected density of states (PDOS) is represented in Figure 3 in which the upper part of the valence band and the conduction band are highlighted. For the TeO_3*(LP)* entity, the contribution of the Te 5*p* states dominate the upper VB with a maximum around -6.5 to -5 eV, while the Te 5*s*, 4*d* states are found with a much smaller contribution in the whole range of the upper VB, and are hybridized with O 2*p* states. Te 5*s*, 4*d* states are found together with O2*p* states in the CB. For the octahedral CoO_6 and CoO_5F_1, the Co 3*d* up (↑) spins are filled while the down (↓) spins are partially empty leading to the probable configuration $(t_2g)\uparrow^3$ $(e_g)\uparrow^2$ $(t_2g)\downarrow^2$ $(e_g)\downarrow^0$. Similarly, CoO_5, with spin(↑) fully occupied and spin(↓) partially empty, is also most probably in the Co^{2+} high spin state.

Focusing on the mixed anion CoO_5F_1, it is interesting to analyze the different contribution of O^{2-} and F^- anions around cobalt. The 2*p* states of fluorine are found with a higher contribution lower in the VB while the O 2*p* states contributes more than F in the upper VB below the Fermi level, as expected for the more covalent character of the Co-O bond compared to Co-F.

As shown in Figure 4, there is barely any difference between the ZFC and FC susceptibility data for **1** except for a small divergence below 20 K, possibly due to the magnetic anisotropy of the Co^{2+} ion. The best-fit values of Curie−Weiss law[46] are C = 3.33 (1) mol^{-1}·K, θ_{CW} = −63.7 (2) K and χ_o=0.014 (1) emu/mol·Oe·Co. The effective magnetic moment is μ_{eff} = 5.15 (2) μ_B per Co^{2+} ion: this value is considerably larger than the spin-only value (3.87 μ_B) expected for high-spin (HS) d^7 Co^{2+} (S = 3/2) ions, which implies a significant orbital contribution for the magnetically anisotropic Co^{2+} ions. The negative value of θ_{CW} suggests the presence of dominant antiferromagnetic exchange interactions *J*. Using the mean-field (MF) formula, we may evaluate

J from the Curie−Weiss temperature: $\theta_{CW} = zJS(S + 1)/3k_B$, where z is the number of the nearest neighbor Co^{2+} spins and k_B is the Boltzmann constant. Here, we take the average value of z = 5.6, based on the fact that Co1 has six nearest neighbors, Co2 has five nearest neighbors, while Co3 has six nearest neighbors. This yields $J_{MF}/k_B \approx -9.1$ K for S = 3/2. The sizable antiferromagnetic exchange interactions are further justified by considering the bond angles between the Co^{2+} ions. The average Co–O–Co bond angle is 105.1°, beyond the range in which ferromagnetic exchange interactions are dominant (90–100°).[47] Moreover, as the Co–F–Co bond angle is 118.2 (1)°, the intermediate strength of the antiferromagnetic coupling is in accordance with the Goodenough–Kanamori–Anderson superexchange rules, which predict that antiferromagnetic interactions become stronger as the bond angles mediating superexchange paths increase towards 180° beyond the crossover angle where the exchange interaction changes its sign from ferromagnetic to antiferromagnetic.

At low temperatures, $\chi(T)$ displays a small kink and a subsequent drop towards zero kelvin, giving an indication of antiferromagnetic ordering. The transition temperature was determined as T_N = 9.6 K by a sharp peak in the derivative of $d(\chi T)/dT$, as plotted in the inset of Figure 4a. λ-type anomalies are also found in the heat capacity of the title phase at temperatures matching well with those where characteristic susceptibility features were determined, see Figure 4c.

From the ratio $f = |J_{MF}/T_N| \sim 1.2$ (1), we infer that **1** has a three-dimensional magnetic structure .

The plot of magnetization *versus* applied field at 2 K is shown in Figure 4b. The magnetization increases linearly up to 4.5 T without detectable hysteresis and subsequently exhibits a steep increase. The former feature is fully consistent with an antiferromagnetic (rather than weakly ferrimagnetic) system and the latter may be due to a spin-flop transition at H_{SF} = 4.5 T.

4. Conclusion

In conclusion, $Co_{15}F_2(TeO_3)_{14}$ obtained by the optimised hydrothermal synthesis concerned with complex mineralization process and redox chemistry, which features an unique structural solution to accommodate Te^{IV} lone pairs in pyritohedron-shaped closed cavities. The magnetic structure is an S=3/2 honeycomblike spin network.

References

(1) Kageyama, H.; Hayashi, K.; Maeda, K.; Attfield, J. P.; Hiroi, Z.; Rondinelli, J. M.;

Poeppelmeier, K. R. Expanding frontiers in materials chemistry and physics with multiple anions. *Nat. Commun.***2018**, *9*, 772.
(2) Kamihara, Y.; Watanabe, T.; Hirano, M.; Hosono, H. Iron-Based Layered Superconductor La[$O_{1-x}F_x$]FeAs (x = 0.05−0.12) with T_c = 26 K. *J. Am. Chem.Soc.* **2008**, *130*, 3296–3297.
(3) Al-Mamouri,M.; Edwards, P. P.; Greaves, C.; Slaski,M. Synthesis and superconducting properties of the strontium copper oxy-fluoride $Sr_2CuO_2F_{2+\delta}$.*Nature* **1994**, *369*, 382–384.
(4) Kim,Y.-I. Woodward, P. M.; Baba-Kishi, K. Z.; Tai, C. W. Characterization of the Structural, Optical, and Dielectric Properties of Oxynitride Perovskites AMO_2N (A = Ba, Sr, Ca; M = Ta, Nb).*Chem. Mater.* **2004**, *16*, 1267–1276.
(5) Kobayashi,Y.; Hernandez, O. J.; Sakaguchi, T.; Yajima,T.; Roisnel, T.; Tsujimoto, Y.; Morita,;M.; Noda, Y.; Mogami,;Y.; Kitada, ;A.; Ohkura,;M.; Hosokawa,;S.; Li,;Z.; Hayashi,;K.; Kusano,;Y.; Kim,J. e.; Tsuji, N.; Fujiwara,;A.; Matsushita,;Y.; Yoshimura,;K.; Takegoshi,;K.; Inoue, M.; Takano M.; Kageyama, H.An oxyhydride of $BaTiO_3$ exhibiting hydride exchange and electronic conductivity**.** *Nat. Mater.* **2012**, *11*, 507-511.
(6) Opik, U.; Pryce, M. H. L. Studies of the Jahn-Teller effect. I. A survey of the static problem. *Proc. R. Soc. London, Ser. A* **1957**, *238*, 425−447.
(7) Pearson, R. G. Symmetry rule for predicting molecular structures**.** *J. Am. Chem. Soc.* **1969**, *91*, 4947−4955.
(8) Zhang, H.; Zhang, M.; Pan, S.; Dong, X.; Yang, Z.; Hou, X.; Wang, Z.; Chang, K. B.; Poeppelmeier, K. R. $Pb_{17}O_8Cl_{18}$: A Promising IR Nonlinear Optical Material with Large Laser Damage Threshold Synthesized in an Open System**.** *J. Am. Chem. Soc.* **2015**, *137*, 8360−8363.
(9) Mao, J.-G.; Jiang, H.-L.; Kong, F. Structures and properties of functional metal selenites and tellurites**.** *Inorg. Chem.* **2008**, *47*, 8498−8510.
(10) Kim, Y.; Lee, D. W.; Ok, K. M. Rich Structural Chemistry in New Alkali Metal Yttrium Tellurites: Three-Dimensional Frameworks of $NaYTe_4O_{10}$, $KY(TeO_3)_2$, $RbY(TeO_3)_2$, and a Novel Variant of Hexagonal Tungsten.*Inorg. Chem.* **2015**, *54*, 389−395.
(11) Johnsson, M.; Törnroos, K. W.; Lemmens, P.; Millet, P. Crystal Structure and Magnetic Properties of a New Two-Dimensional S = 1 Quantum Spin System $Ni_5(TeO_3)_4X_2$ (X = Cl, Br)**.** *Chem.Mater.* **2003**, *15*, 68−73.
(12) Dutreilh, M.; Thomas, P.; Champarnaud-Mesjard J.-C.; Frit, B. Crystal structure of a new gallium tellurite: $Ga_2Te_4O_{11}$**.** *Solid State Sci.* **2001**, *3*, 423–431.
(13) Chen, Y.-G.; Yang, N. Yao, X.-N.; Li, C.-B. Guo, Y.; Zhang X.-M. Synergetic Influence of Alkali-Metal and Lone-Pair Cations on Frameworks of Tellurites**.** *Inorg. Chem.* **2018**, DOI: 10.1021/acs.inorgchem.8b00266.
(14) Johnston M. G.; Harrison, W. T. A. Lone-Pair Self-Containment in Tellurite Tubes: Hydrothermal Syntheses and Structures of $BaTe_3O_7$ and $BaTe_4O_9$**.** *J. Am. Chem. Soc.* **2002**, *124*, 4576–4577.
(15) Hu, S.; Johnsson, M.; Law, J. M.; Bettis, J. L.; Whangbo, M.-H.; Kremer, R. K.Crystal Structure and Magnetic Properties of $FeSeO_3F$ Alternating Antiferromagnetic S = 5/2 chains**.** *Inorg. Chem.* **2014**, *53*, 4250−4256.
(16) Pregelj, M.; Zaharko, O.; Zorko, A.; Kutnjak, Z.; Jeglic, P.; Brown, B. P.; Jagodic, Z.; Berger, H.; Arcon, D. Crystal Structure and Magnetic Properties of the $S = {}^1/_2$ Quantum Spin System $Cu_7(TeO_3)_6F_2$ with Mixed Dimensionality**.** *Phys. Rev. Lett.* **2009**,*103*, 147202(4).
(17) Johnsson, M.; Törnroos, K. W.; Mila, F.; Millet, P. Tetrahedral Clusters of Copper(II): Crystal Structures and Magnetic Properties of $Cu_2Te_2O_5X_2$ (X = Cl, Br)**.** *Chem. Mater.* **2000**, *12*, 2853−2857.
(18) Becker, R.; Johnsson, M.; Kremer, R. K.; Klauss, H.-H.; Lemmens, P. Crystal Structure and

Formatted: English (United Kingdom)
Formatted: English (United Kingdom)
Formatted: English (United Kingdom)

Magnetic Properties of $FeTe_2O_5X$ (X = Cl, Br): A Frustrated Spin Cluster Compound with a New Te(IV) Coordination Polyhedron**.** *J. Am. Chem. Soc.* **2006**, *128*, 15469−15475.

(19) Takagi, R.; Johnsson, M.; Gnezdilov, V.; Kremer, R .K.;Brenig, W.; Lemmens, P. Investigation of the oxohalide $Cu_4Te_5O_{12}Cl_4$ with weakly coupled tetrahedra. *Phys. Rev. B* **2006**, *74*, 0144131–0144138.

(20) Zhang. D.; Johnsson, M.; Berger, H.; Kremer, R. K.; Wulferding, D.; Lemmens, P. Separation of the Oxide and Halide Part in the Oxohalide $Fe_3Te_3O_{10}Cl$ Due to High Lewis Acidity of the Cations**.** *Inorg. Chem.* **2009**, *48*, 6599–6603.

(21) Laval, J. P.; Boukharrata, N. J. New vanadium(IV) and titanium(IV) oxyfluorotellurates(IV): $V_2Te_2O_7F_2$ and $TiTeO_3F_2$**.** *Acta Crystallogr*. **2009**, *C65*, i1.

(22) Laval, J. P.; Boukharrata, N. J.; Thomas, P.New oxyfluorotellurates(IV): $MTeO_3F$ (M = Fe^{III}, Ga^{III} and Cr^{III})**.** *Acta Crystallogr*. **2008**, *C64*, i12.

(23) Hu, S.; Johnsson, M. Synthesis and crystal structure of two synthetic oxofluoride framework compounds–$Co_2TeO_3F_2$ and $Co_2SeO_3F_2$**.** *Dalton Trans.* **2012**, *41*, 12786−12789.

(24) *SAINT: Area-Detector Integration Software*; Siemens Industrial Automation, Inc.: Madison, **1996**.

(25) *SADABS: Area-Detector Absorption Correction*; Siemens Industrial Automation, Inc.: Madison, **1995**.

(26) G. M. Sheldrick, A short history of SHELX**.** *Acta Cryst*. **2008**, A64, 112–122.

(27) G. M. Sheldrick, Crystal structure refinement with SHELXL**.** *Acta Cryst*. **2015**, C71, 3–8.

(28) Yahia, H.;B. Shikano, M.; Kobayashi ,H. Single crystal growth of the novel $Mn_2(OH)_2SO_3$, $Mn_2F(OH)SO_3$, and $Mn_5(OH)_4(H_2O)_2[SO_3]_2[SO_4]$ compounds using a hydrothermal method.*Dalton Trans*, **2013**, *42*, 7158-7166.

(29) Fedotov, S. S.; Khasanova, N.R.; Samarin, A. S.; Drozhzhin, O. A.; Batuk, D.; Karakulina, O. M.; Hadermann, J.; Abakumov, A. M.; Antipov, E. V. $AVPO_4F$ (A = Li, K): A 4 V Cathode Material for High-Power Rechargeable Batteries**.** *Chem. Mater*. **2016**, *28*, 411-415.

(30) Kresse, G.; Hafner, J. Ab initio molecular dynamics for liquid metals**.** *Phys. Rev. B* **1993**, *47*, 558.

(31) Kresse, G.; Furthmüller, J. Efficiency of ab-initio total energy calculations for metals and semiconductors using a plane-wave basis set**.** *Comput. Mater. Sci.* **1996**, 6, 15.

(32) Kresse, G.; Furthmüller, J. Efficient iterative schemes for *ab initio* total-energy calculations using a plane-wave basis set**.** *Phys. Rev. B* **1996**, *54*, 11169.

(33) Perdew, J. P.; Burke, K.; Ernzerhof, M. Generalized gradient approximation made simple**.** *Phys. Rev. Lett.* **1996**, *77*, 3865.

(34) Dudarev,S. L.; Botton,G. A.; Savrasov, S. Y.; Humphreys, C. J.; Sutton,A. P. Electron-energy-loss spectra and the structural stability of nickel oxide: An LSDA+ U study**.** *Phys. Rev. B* **1998**, 57, 1505.

(35) Silvi, B.; Savin, A. Classification of chemical bonds based on topological analysis of electron localization functions**.** *Nature* **1994**, *371*, 683–686.

(36) Brese, N. E.; O'Keeffe, M. Bond-valence parameters for solids.*Acta Crystallogr.* **1991**, *B47*, 192–197.

(37) Kohn**,** K.; Inoue**,** K.**;** Horie**,** O.; Akimoto**.** S.I.Crystal chemistry of $MSeO_3$ and $MTeO_3$ (M= Mg, Mn, Co, Ni, Cu, and Zn). *J. Solid State Chem.* **1976**, *18*, 27–37.

(38) Addison, A. W.; Rao, N. T.; Reedijk, J.; van Rijn, J.; Verschoor, G. C. Synthesis, structure, and spectroscopic properties of copper(II) compounds containing nitrogen–sulphur donor ligands; the crystal and molecular structure of aqua[1,7-bis(*N*-methylbenzimidazol-2′-yl)-2,6-dithiaheptane]copper(II) perchlorate. *J. Chem. Soc., Dalton Trans*. 1984, 1349–1356.

Formatted: English (United Kingdom)

Formatted: English (United Kingdom)

Field Code Changed

Field Code Changed

Formatted: English (United Kingdom)

(39) Seddon, J.; Suard, E.; Hayward, M. A. Topotactic Reduction of $YBaCo_2O_5$ and $LaBaCo_2O_5$: Square-Planar Co(I) in an Extended Oxide**.** *J. Am. Chem.Soc.* **2010**, *132*, 2802–2810.
(40) Lee, D. W.; Bak, D.-b.; Kim, S. B.; Kim, J.; Ok, K. M. Effect of the Framework Flexibility on the Centricities in Centrosymmetric $In_2Zn(SeO_3)_4$ and Noncentrosymmetric $Ga_2Zn(TeO_3)_4$**.** *Inorg. Chem.* **2012**, *51*, 7844–7850.
(41) Brown, I. D. Bond valence as an aid to understanding the stereochemistry of O and F complexes of Sn (II), Sb (III), Te (IV), I (V) and Xe (VI). *J. Solid State Chem.* **1974**, *11*, 214–233.
(42) Irvine, J. T. S.; Johnston, M. G.; Harrison, W. T. A. Lone-pair containment in closed cavities. The MTe_6O_{13} (M= Mn, Ni, Co) family of ternary oxides. *Dalton Trans*. **2003**, 2641–2645.
(43) Smith, A. E.; Mizoguchi, H.; Delaney, K.; Spaldin ,N. A.; Sleight, A. W.; Subramanian, M. A. Mn^{3+} in Trigonal Bipyramidal Coordination: A New Blue Chromophore. *J. Am. Chem. Soc.* **2009**, *131*, 17084–17086.
(44) Foglio, M.E.; Barberis, G.E.Study of Co^{2+}in different crystal field environments. Braz. J. Phys. 2006, *36(1A)*, 40-54.
(45) Rojo,J.M.; Fernández,J.R.; Fernández-Díaz, M.T.; Rojo, T. Sinusoidal magnetic structure in a three-dimensional antiferromagnetic $Co_2(OH)AsO_4$: Incommensurate-commensurate magnetic phase transition. *Phys. Rev. B* 2010, *81*, 134431.
(46) In the high-temperature paramagnetic region, the magnetic susceptibility approximated to M/H could be fitted by a Curie−Weiss law $\chi(T) = C/(T - \theta_{CW}) + \chi_o$, where C is the molar Curie constant and θ_{CW} is the Curie–Weiss temperature. The χ_o term contains temperature-independent contributions stemming from the diamagnetism of the core electron shells and the van Vleck paramagnetism of the Co^{2+} ions.
(47) Du, M.; Guo, Y.-M.; Bu, X.-H.; Ribas J. Ligand Design for Alkali-Metal-Templated Self-Assembly of Unique High-Nuclearity Cu^{II} Aggregates with Diverse Coordination Cage Units: Crystal Structures and Properties. *Eur. J. Inorg. Chem.* **2004**, 3228-3231.

Formatted: English (United Kingdom)
Formatted: English (United Kingdom)
Field Code Changed
Formatted: English (United Kingdom)
Formatted: English (United Kingdom)

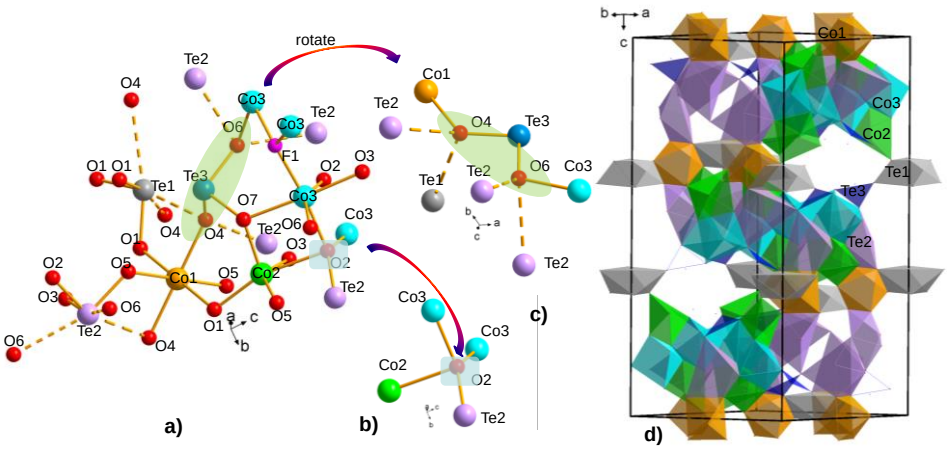

Figure 1: a) View of a fragment of the crystal structure of **1** showing the cation coordination environments and atom labelling. The long Te–O bonds are shown as dashed lines (see text); b) detail of the O2 coordination environment; c) detail of the O6 coordination environment. d) Projection of the structure of 1 along the [110] direction.

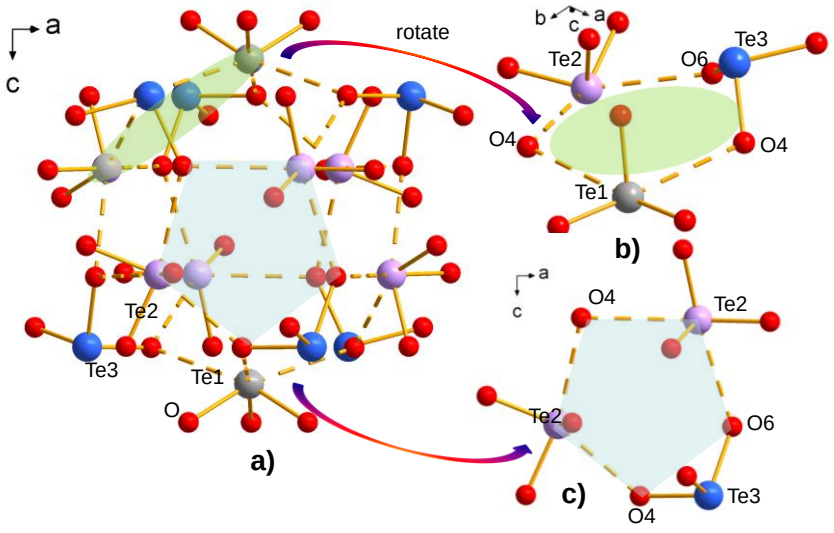

Figure 2: a) view down [010] of a $[(TeO_3)_{14}]^{28-}$ building unit, which encloses a pyritohedral cavity made up of twelve distorted pentagonal faces (one shaded light blue), each of which is formed from a trio of TeO_3 groups (green circle); b) expanded view of a trio of TeO_3 groups; c) expanded view of the pentagonal face Te2/O4/Te2/O6/O4 with O4···O6 as one edge and the Te3 atom as a "handle". The lone pairs of the Te1 and Te2 atoms point into the cavity, which has atom-to-atom dimensions of ~4.3 Å × ~4.3 Å.

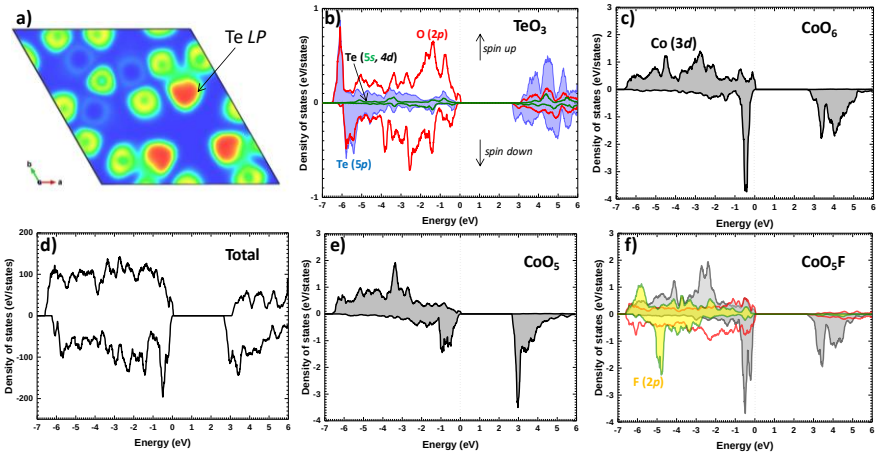

Figure 3. a) Slice of the DFT calculated valence Electron Localization Function (ELF) for $Co_{15}F_2(TeO_3)_{14}$ with blue corresponding to weak localization and orange to complete localization (lone pairs). Projected density of states (PDOS) focusing on TeO_3 (b), CoO_6 (c), CoO_5 (e), CoO_5F entities and total density of states (f).

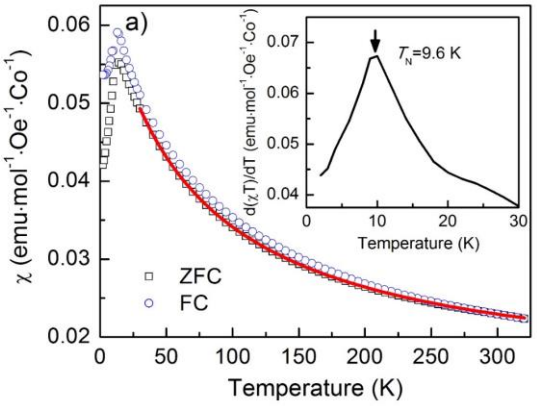
a)
χ (emu·mol-1·Oe-1·Co-1)
Temperature (K)
ZFC
FC
d(χT)/dT (emu·mol-1·Oe-1·Co-1)
TN=9.6 K
Temperature (K)

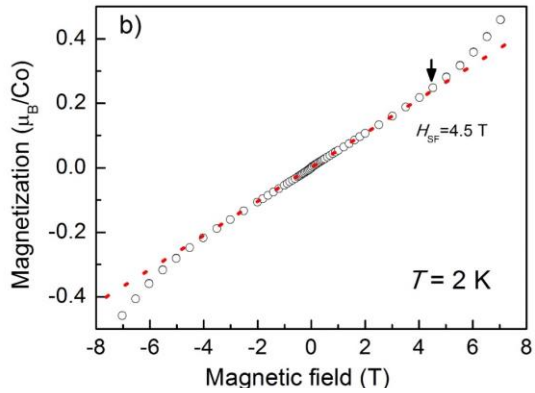
b)
Magnetization (μB/Co)
Magnetic field (T)
HSF=4.5 T
T= 2 K

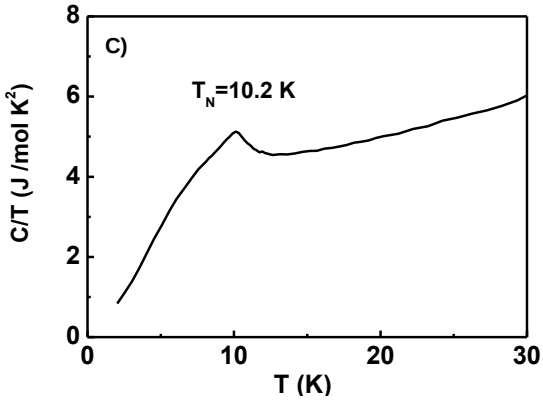
C)
TN=10.2 K
C/T (J /mol K2)
T (K)

Figure 4: (a) The magnetic susceptibility of **1** measured under an external field of H = 200 Oe in the temperature range of 2–320 K. The solid line is a Cuire–Weiss fit. The inset shows the derivative of $\chi(T)$ *versus* T at low temperatures, indicating the onset of antiferromagnetic ordering at T_N = 9.6 K. (b) Magnetization isotherm measured at T = 2 K. The dashed line is a fit to a linear dependence of the magnetization; the arrow indicates the onset of the proposed 'spin-flop' transition. (c) Specific heat of $Co_{15}F_2(TeO_3)_{14}$.

Table 1. Crystal data, measurement parameters and structural refinement parameters of $Co_{15}F_2O_{42}Te_{14}$ at room temperature.

	$CsMn_3F_6(SeO_3)_2$
Molar weight (g/mol)	3380.35
Symmetry	trigonal
Space group	$R\bar{3}$
a (Å)	11.6649 (4)
c (Å)	27.3173 (10)
V (Å^3)	219.1 (3)
μ (mm^{-1})	15.084
R(int) (%)	2.55
indep all (I > 2σ(I))	1776
indep obsd (I > 2σ(I))	1665
Number of refined parameters	113
$R(F)^a$[I > 2σ(I)/all data, %]	2.23/2.52
R_w (F^2)^b [I > 2σ(I)/all data,	4.45/4.53

$^aR = \sum \| F_o| - |F_o \| / \sum |F_o|$, $^bR_w = [\sum w(|F_o^2| - |F_c^2|)^2 / \sum w|F_o^2|^2]^{1/2}]$

Highlight

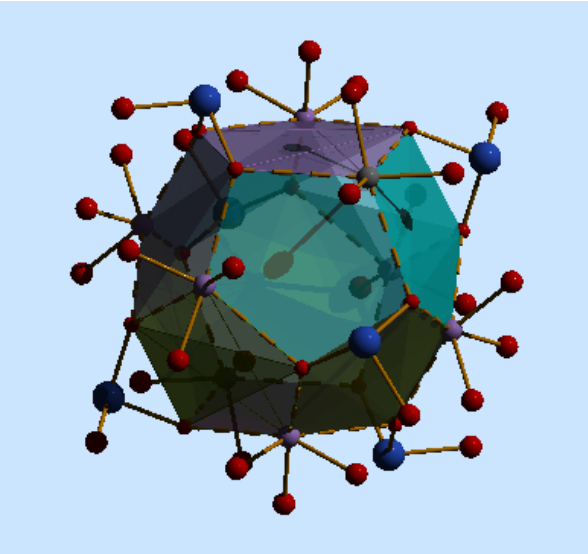

Optimised hydrothermal synthesis concerned with complex mineralization process and redox chemistry has allowed the first synthesis of $Co_{15}F_2(TeO_3)_{14}$, of the important fluoride tellurites. The structure features an extremely rare example of the Te(IV) lone pairs self-containment in pyritohedron-shaped $[(TeO_3)_{14}]^{28-}$ units, which contains grossly distorted TeO_{3+3} octahedra and planar trimeric CoO_5F octahedra jointed by the central fluorine atom novel building blocks.